



university of
 groningen

faculty of mathematics and
 natural sciences

zernike institute for
 advanced materials

Low-energy electron-induced chemistry of PMMA

A thesis presented for
The partially fulfillment of the degree of:
Master of Science in Nanoscience

Bo Sun
S2234882

Supervisors:
dr. ir. W.F. van Dorp
prof. J.T.M. De Hosson

July 2014

Abstract

Poly-methyl methacrylate (PMMA) has been extensively studied in the past decades as a photoresist in lithography industry. To achieve sub-micron resolution, the resist is usually exposed to electrons having a high energy of 10 – 100 keV. Secondary electrons generated from the primary electrons are believed to play an important role in the modification of the resist. However, most of the studies do not distinguish explicitly between the effects of the primary electrons and that of low-energy secondary electrons. Few experimental studies have been done on the effects of low-energy electrons on PMMA.

In this master project we investigated the low-energy electron-induced chemistry on photoresist PMMA with 5 – 50 eV electrons. The ion fragments that come off the film during irradiations as well as the film thickness and photoelectron spectra before and after the irradiations are investigated, using mass spectroscopy (MS), X-ray photoelectron spectroscopy (XPS) and atomic force microscopy (AFM). An energy threshold of around 21 – 27 eV is found for the low-energy electron-induced reactions of PMMA. An explanation based on charging is given for this relatively high threshold comparing to other studies. The reaction process of dissociation of PMMA by low-energy electrons is discussed and direct ionization is believed to be the most likely mechanism. No evidence of dissociative electron attachment (DEA) is found in the process. At high dose of low-energy electrons, the PMMA crosslinks as its for high-energy irradiations.

Table of Contents

Abstract	3
Table of Contents	4
1. Introduction	5
2. Background	8
2.1. Low-energy electron-induced chemistry.....	8
2.2. Electron-induced chemistry on PMMA	12
3. Experimental setup and methods	19
3.1. Experimental setup	19
3.2. Materials used	21
3.3. Preparation of PMMA thin films	21
3.4. Low-energy electron irradiation	22
3.5. Development.....	23
3.6. AFM measurement.....	23
4. Results and discussions	24
4.1. Threshold energy of exposure	24
4.2. Decomposition of PMMA by low-energy electrons.....	28
4.3. Crosslinking of PMMA.....	34
4.4. Charging effects on PMMA thin films	36
5. Conclusions	40
6. References.....	41
7. Acknowledgement.....	43

1. Introduction

The feature size of electronic circuits shrinks every year, roughly according to “Moore’s Law”. By the year 2020, the International Technology Roadmap for Semiconductors foresees that the half pitch of flash memory is miniaturized to 10 nm. Because of this small dimension, the standard lithography technique that using ultra violet (UV) light cannot meet the requirements for future chip manufacture. Among the predicted technologies that could be optimized for future use, extreme ultraviolet lithography (EUVL) is the most promising approach, using extreme ultraviolet (EUV) light with a wavelength of 13.5 nm. A schematic drawing of EUVL is shown in Fig. 1.

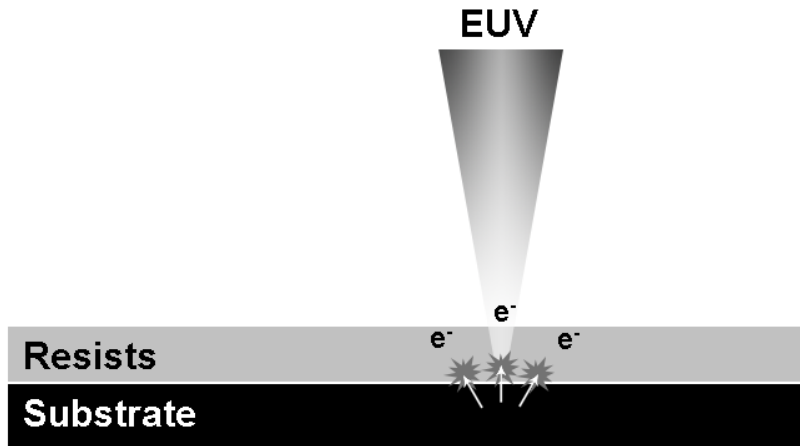


Fig. 1. A schematic drawing of secondary electrons generated in EUV lithography.

Generally in industrial lithography, a resist (a photo-sensitive layer) is used to transfer patterns from a mask onto a Si wafer. While EUV light exposes the resist through photon-induced chemistry, EUV light is ionizing. This involves a paradigm shift in the technology and implies that a fundamentally different mechanism is now responsible for exposing the resist. The ionizing radiation releases secondary electrons from the substrate that react with the resist. It is believed that these secondary electrons also play an important role. For example bond scission of a polymer resist can be enabled by low-energy secondary electrons via a chemical process known as dissociative electron attachment (DEA) [1]. It has been estimated that about four secondary electrons on average are generated by one EUV photon [2]. As Fig. 2 shows, the inelastic mean free path of these low-energy secondary electrons first decreases as the electron energy increases because a faster electron has a shorter interaction time with matter and therefore a lower probability of interacting, until it reaches a minimum around 15 eV. Then it increases again above 15 eV because the number of available interaction channels increases [3].

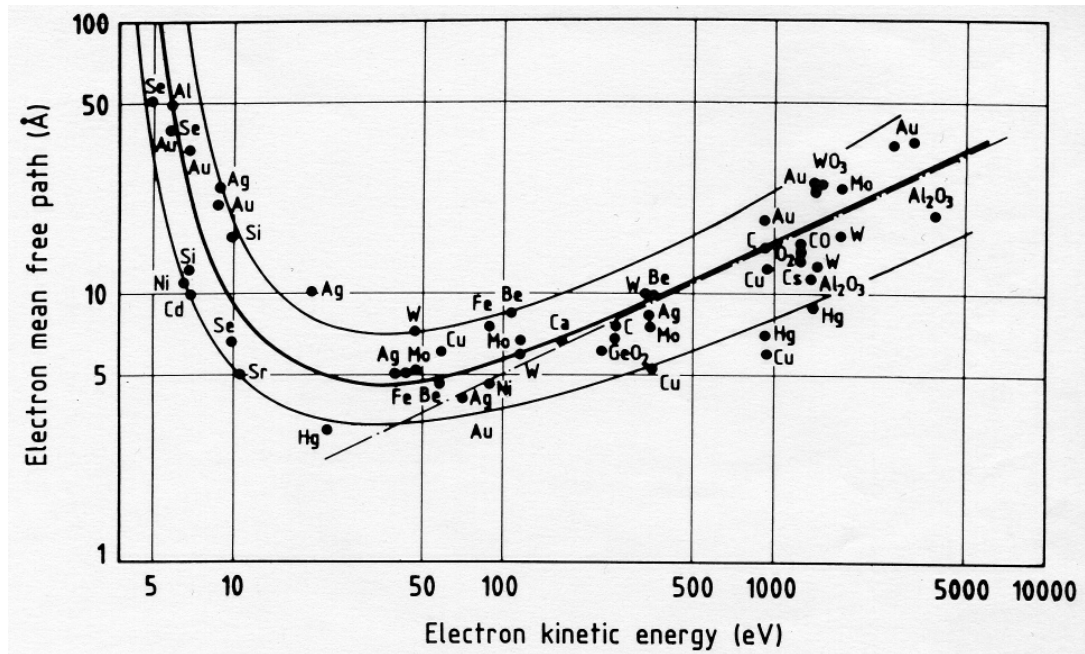


Fig. 2. Universal electron mean free path profile in different materials. [3]

The inelastic mean free path of electrons with energies in the range of few of eV is well above 1 nm. If indeed the secondary electrons are one of the dominant components in exposing the resist, this mean free path will limit the ultimate resolution of EUV resists. To optimize the resist materials used in semiconductor lithography, a fundamental understanding of how the low-energy electrons interact with resists is needed.

Poly-methyl methacrylate (PMMA) is a well-known resist for UV, electron and X-ray lithography. However, most of the studies on PMMA irradiation chemistry do not distinguish explicitly between the effects of high-energy primary irradiation and those of low-energy secondary electrons. While it is widely assumed that low-energy electrons play an important role in the chemistry, little is known about the background. The only work that studies the effects of low-energy electron (10 – 50 eV) irradiation on PMMA thin films was reported by Bermudez [4]. The study is based on polarization-modulated infrared reflection absorption spectroscopy (IRRAS). A reduction of intensities of the bands associated to the ester group is found at certain dose which is similar to results from Raman spectroscopy [5]. Degassing is also observable via mass spectroscopy, leading to an erosion of materials, which is evident from the decrease in intensity of the whole mid-IR range in IRRAS spectrum. The results suggest that low-energy electrons appear to damage PMMA in the same manner as more energetic forms of radiation, but the fundamental model of the underlying mechanism is still missing.

Assoc Prof. S. J. van der Molen and dr. Aniket Thete at the Leiden University studied the energy dependence of low-energy electron-induced chemistry on PMMA using low-

energy electron microscopy (LEEM). Point exposures on a spin-coated PMMA thin film reveals that there is a threshold of 18 eV for the energy of the electrons exposing the thin film. Above the threshold the exposed areas can be developed, while below the threshold they cannot. The results obtained in this thesis will be compared to the results obtained by LEEM.

In this thesis the electron interaction with PMMA resist is studied. We will mainly focus on investigating the chemical change of PMMA before and after exposure and development by using mass spectroscopy, X-ray photoelectron spectroscopy, and atomic force microscopy. Gas phase data will be analyzed as well as the thickness of the films before and after development to determine how these low-energy electrons (1- 50 eV) interact with PMMA thin films. These results will be compared to the mentioned experimental results. Combined, they can offer useful information and solution to the improvement of PMMA and other polymer resists by providing the fundamental knowledge of low-energy electron-induced chemistry.

Chapter 2 describes the background of low-energy electron-induced chemistry in general and the background of low-energy electron-induced chemistry of PMMA. Some literatures concerning the works on low-energy electron-induced chemistry and electron-induced chemistry of PMMA are shown and discussed.

Chapter 3 shows the details regarding the experimental setup and materials used in our experiments, as well as the experiments details on the sample preparation, development and thickness measurements using atomic force microscopy.

Chapter 4 shows our results from the measurements acquired by mass spectroscopy, X-ray photoelectron spectroscopy and atomic force microscopy. The results are compared to the literatures described in chapter 2, based on which a mechanism is suggested.

Chapter 5 summarizes the conclusions.

2. Background

2.1 Low-energy electron-induced chemistry

High-energy radiation plays an important role in variety of applications including plastics processing, food preservation and medical examinations. Especially in lithography, high-energy radiation is the main source for modifying the resists thus enabling the production of integrated circuits in electronic devices. However, the radiation-induced processes are not less well controlled in lithography than the primary radiations, which have a very high precision. It is because an abundance of secondary electrons is generated via inelastic scattering between radiation and matter. The secondary electrons are the major driving forces in most radiation-induced chemistry, other than the primary irradiation. They are responsible for the production of reactive species such as free radicals.

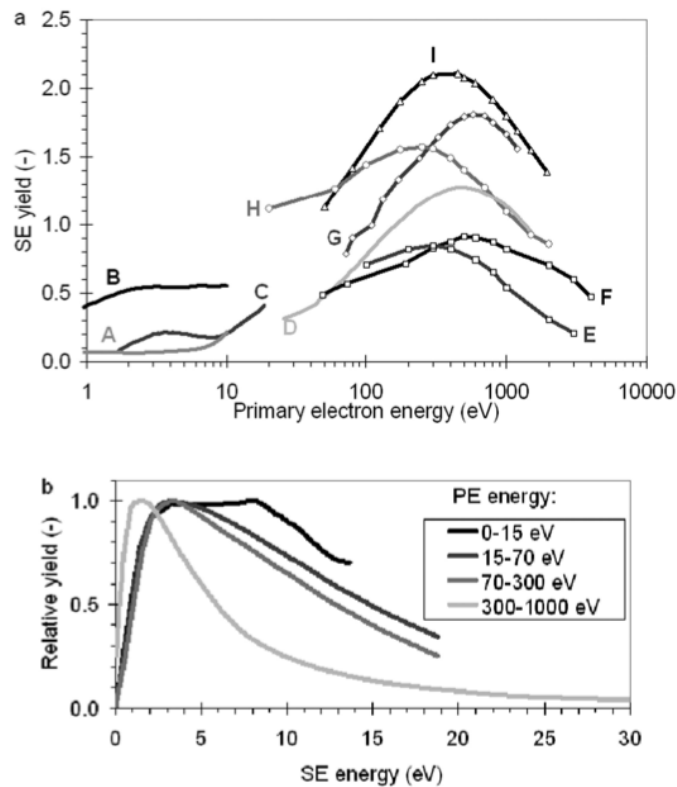


Fig. 3. (a) The energy distribution of secondary electrons generated by various materials: copper (A), copper after exposure to air (B), molybdenum (C), nickel (D), carbon (E), molybdenum (F), platinum (G), copper (H) and copper (I). (b) The SE spectrum as a function of incident electron energy for platinum (0 eV - 300 eV) and copper (300 eV - 1000 eV). [6]

Fig. 3 (a) shows the energy distribution of secondary electrons generated by various materials as function of electron exposure. A general trend can be found that as the primary electron energy increases the secondary electron yield first increase and reaches a maximum at different energies around 300 – 800 eV. At even higher dose the yield drops as the primary electron energy increases. Comparing (A) to (B) the secondary electron yields is higher for copper after exposure to air, indicating that oxidized/not clean surfaces contribute to the higher yields. Fig. 3 (b) shows the typical spectrum for secondary electrons generated by platinum at different primary electron energies. At low primary electron energies (0 – 15 eV) most of the secondary electrons generated have energy between 3 – 10 eV. As the primary electron energies increase the maximum of the spectrum shift to lower energies. At primary energies above 300 eV, most of the secondary electrons have energy between 0.8 – 3 eV.

When low-energy electrons interact with molecules, a variety of reaction pathways are possible [1]. Due to inelastic scattering processes, the electrons can ionize, excite, and/or dissociate the molecules. There are three primary channels for reactions between low-energy electrons and atoms or molecules in the energy range 0-15 eV: electron impact excitation, electron impact ionization, and electron attachment. Fig. 4 summarizes the electron-induced dissociation pathways of a generic molecule AB.

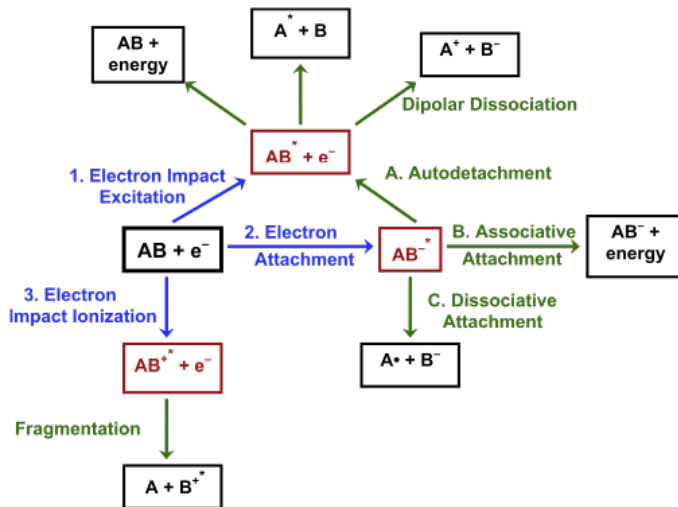


Fig. 4. Electron-induced fragmentation pathways for a generic diatomic molecule AB. [1]

Electron impact excitation and electron impact ionization are non-resonant direct scattering processes, characterized by a smooth increase of electron-induced reaction yield with no maxima. When an electron impinges on a molecule, an excited neutral or ion is formed with electron impact excitation and electron impact ionization, respectively. In both cases the excited state may relax or fragment, resulting in dissociation. The

energies for both cases have onsets, which are the ionization threshold (~ 10 eV) and the excitation threshold (~ 6 eV).

Electron attachment is a resonant scattering process, characterized by a maximum in the function of electron-induced reaction yield at specific energies. When a molecule captures an incoming low-energy electron, an anion is formed which is called transient negative ion (TNI). This occurs at low electron energies between 0-15 eV. The TNI subsequently dissociates into molecular or energy fragments through one of the pathways, such as autodetachment, associative attachment, or dissociative attachment.

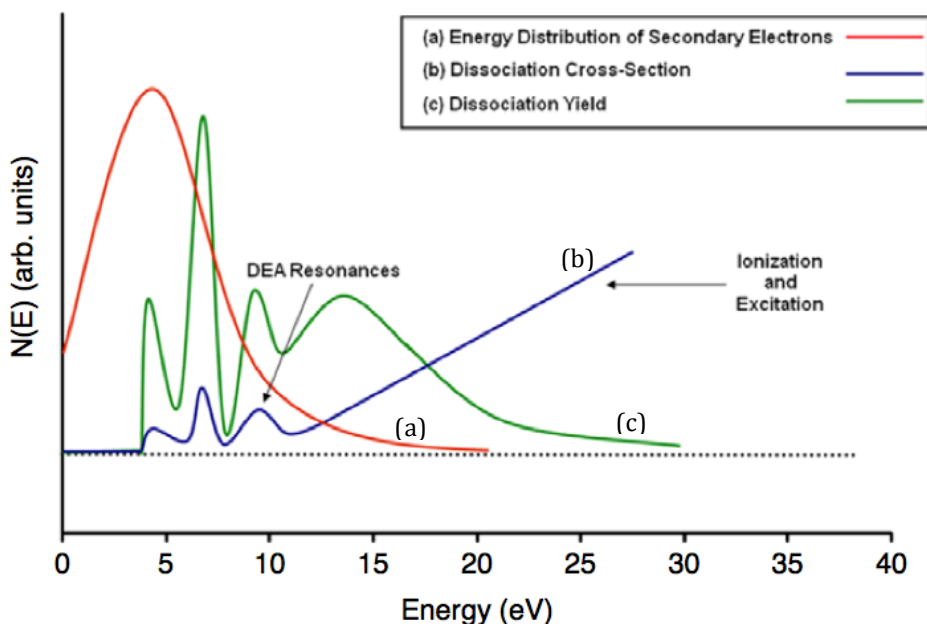


Fig. 5. Schematic of (a) energy distribution of secondary electrons generated by ionization, (b) cross-section for a typical molecule for electron-induced dissociation, and (c) Dissociation yield as a convolution of (a) and (b). [1]

Fig. 5 (a) shows a schematic drawing of the low-energy-electron-induced dissociation yield. Fig. 5 (b) shows the resonance and non-resonance scattering cross section of a typical molecule. At lower energy (< 10 eV) resonance scattering of dissociative electron attachment (DEA) dominates the dissociation; at higher energy (> 10 eV) non-resonance scattering including ionization and excitation becomes the main process. If the energy distribution of secondary electrons generation is considered, the convolution of two curves produces the dissociation yield of secondary electrons for all energy as shown in Fig. 5 (c). Several peaks from DEA remain and a broad maximum for non-resonance scattering shows up. These peaks indicate the energy that contributes most to dissociation.

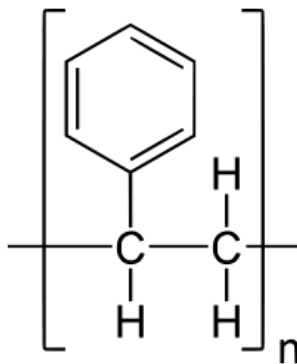


Fig. 6. The repeating unit of polystyrene.

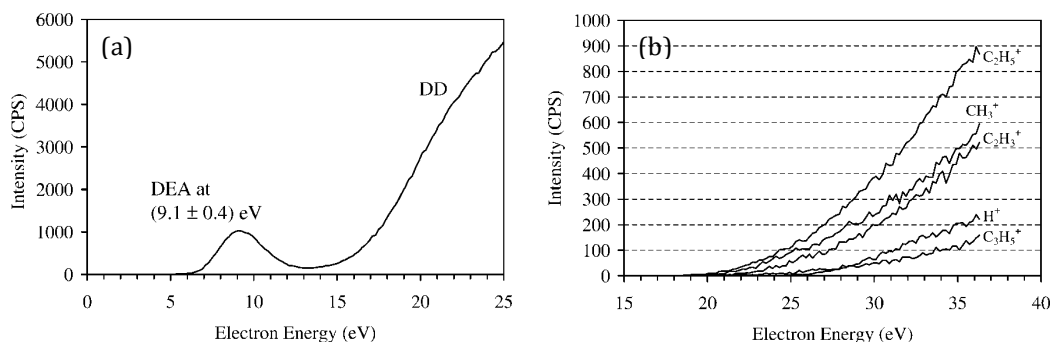


Fig. 7. (a) Energy dependence of the H⁻ ion yield from the exposure of polystyrene (PS) with 5 – 25 eV electrons. (b) Energy thresholds of the predominant positive ions.

Massey et al [7] studied the low-energy electron-induced chemistry of polystyrene via mass spectroscopy using 0 – 100 eV electrons. The chemical structure of polystyrene is shown in Fig. 6. At positive ion mode, the H⁻ ion yield is scanned and the results are shown in Fig. 7 (a). A maximum, which is associated with DEA, is observed around 9.1 eV. Above this maximum at an energy range of 13 – 25 eV, the yield increases monotonically with energy. This increase is attributed to dipolar dissociation because it is the only non-resonant process that can create a stable anion and cation. In negative ion mode, they found that the positive ions emitted from the sample include H⁺, CH₃⁺, C₂H₃⁺, C₂H₅⁺, and C₃H₅⁺. These ions are the products of the direct fragmentation of the main backbone of the polymer. They measured the energy thresholds for this process. Fig. 7 (b) shows the emitted positive ion yields as function of the irradiating electron energy. For all given ions except for H⁺, the thresholds are around 20 – 23 eV. While for H⁺ the threshold is a bit higher (around 25.9 eV). They explain the results by assuming the recombination of positive ions with hydrogen atoms before the emission of positive ions. Below the H⁺ energy threshold of 25.9 eV, cleavage of the C-H bond is possible, but there is not enough energy for the ions to be emitted. At energy lower than 20 eV, only the loss of hydrogen is measured in anion mode, indicating that 20 eV is the threshold for the main chain fragmentation.

2.2 Electron-induced chemistry on PMMA

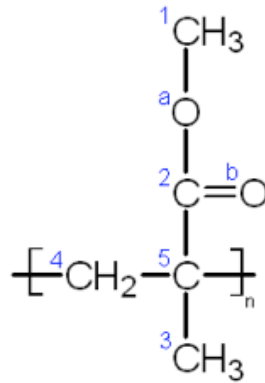
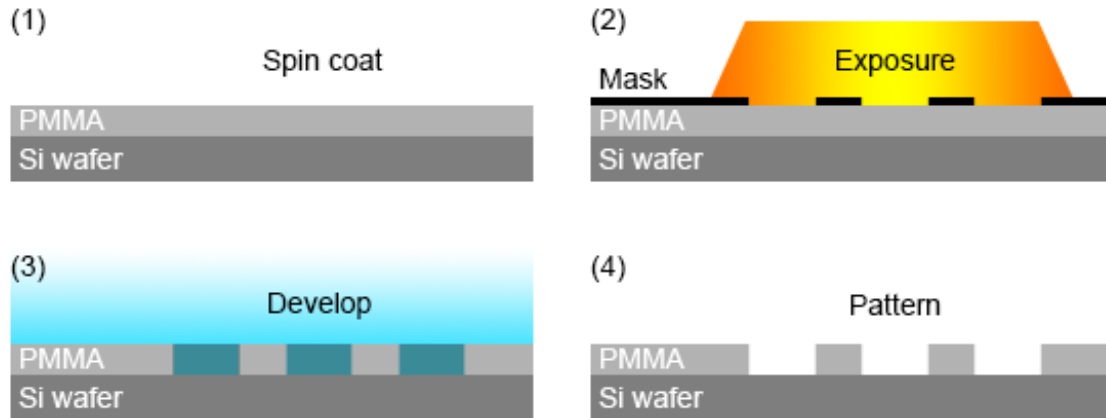


Fig. 8. Molecular structure of PMMA with notations of different carbon (1-5) and oxygen (a, b) atoms.

PMMA (poly-methyl methacrylate) is a thermoplastic polymer. Its molecular structure is shown in Fig. 8 with notations for different carbon and oxygen atoms. It has a glass transition temperature at 105 C, which makes PMMA a stable material at room temperature. PMMA transmits to visible and near infrared and only absorbs UV light having wavelengths below about 300 nm. PMMA is one of the first materials developed to function as electron beam lithography (EBL) resist. Now it is used as a high-resolution polymer resist in X-ray lithography and deep ultra violet lithography (DUVL). It is usually used with molecular weights ranging from 50K to 950K, in a casting solvent such as chlorobenzene or anisole. Such long chains of PMMA do not typically have branches and are not cross-linked, but easily absorb water from the atmosphere.

In a typical lithography procedure, PMMA with varying molecular weights is dissolved in casting solvents, spun onto Si wafers and baked at 170 – 200 °C for 1 – 2 hours. A uniform layer of PMMA is formed after baking and ready for electron exposure. A patterned exposure breaks the polymer into fragments of lower molecular weights that can be dissolved by polymer developers such as MIBK. A schematic drawing of using PMMA as a positive tone resist is shown in Fig. 9.



Positive tone resist PMMA

Fig. 9. A schematic drawing of usage of PMMA as a positive tone resist.

Ennis et al [8] experimentally studied (using mass spectrometry, infrared spectrometry and UV-vis spectrometry) and theoretically simulated the electron-induced degradation of PMMA and proposed its mechanism. They found that large amounts of molecular hydrogen, carbon monoxide and carbon dioxide desorbed during a 3-hour irradiation with 5 keV electrons at 300K as shown in Fig. 10. Two dissociation pathways are possible, which are shown in Fig. 11. An increase in absorption above 250 nm in UV-vis transitions indicates that a conjugated system is newly formed due to Pi-Pi* transition, caused by the dissociation of the carboxylate group and the release of a hydrogen atom.

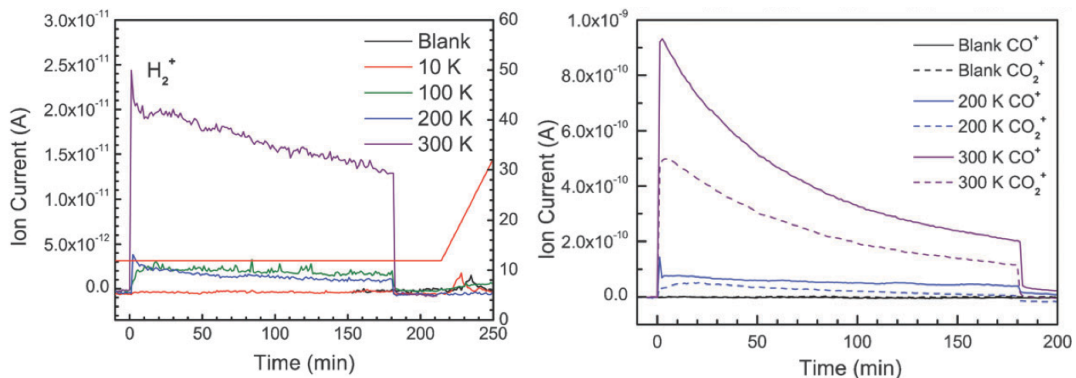


Fig. 10. Ion count for singly ionized hydrogen (H_2^+), carbon monoxide (CO^+) and carbon dioxide (CO_2^+) released from PMMA films irradiated with energetic electrons at 10, 100, 200 and 300 K over the 3 h irradiation period. [8]

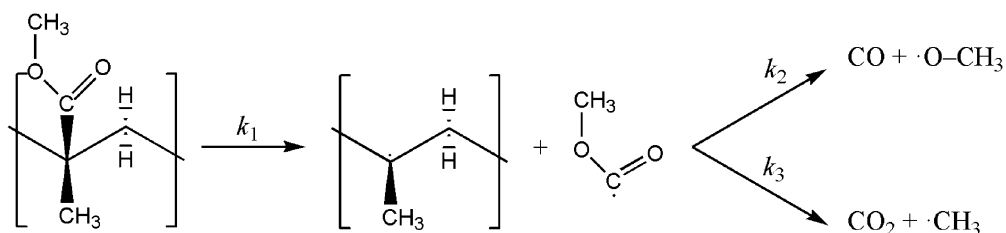


Fig. 11 Dissociation of the ester group followed by two possible dissociation pathways of ester group. [8]

Bermudez has studied the low-energy electron-induced effects on PMMA resist films. Polarization-modulated infrared reflection absorption spectroscopy (IRRAS) has been used to study how the chemical bonds are affected by the low-energy electron irradiation. Fig. 12 (a, b) shows the $\nu(\text{C}=\text{O})$ band of the PMMA before and after irradiation with 50 eV electrons at 225K and 300K, respectively. It shows that in IRRAS the peak corresponding to the $\nu(\text{C}=\text{O})$ band broadens asymmetrically after irradiation at 225K, whereas the net loss of intensity of $\nu(\text{C}=\text{O})$ band is seen after irradiation at 300K. Fig. 12 (c, d) shows the difference spectra at 225K and 300K obtained by subtracting the un-irradiated data from the irradiated data for 50 eV electrons. The positive-going features indicate the irradiation product, while the negative-going features show loss of intensities after irradiation. In Fig. 12 (c) there are positive-going features around 1260, 1380 and 1720 cm^{-1} . The 1260 cm^{-1} feature corresponds to the vibration of the ester group, and the 1720 cm^{-1} feature corresponds to the $\nu(\text{C}=\text{O})$ vibration. In Fig. 12 (d) at 300K all modes suffer roughly the same fractional loss in intensity, indicating an erosion of the PMMA. These results suggest that the ester group is eliminated by the irradiation at 300K with 50 eV electrons. Experiments with lower dose are also done with 10 eV electrons. However the signal-to-noise ratio is much lower than results from 50 eV electrons. A similar but much weaker results are found as compared to Fig. 12 (c, d). It is not clear that whether it is due to the lower dose or lower energy. Results from 50 eV provide evidence to the proposed mechanism in Fig. 11.

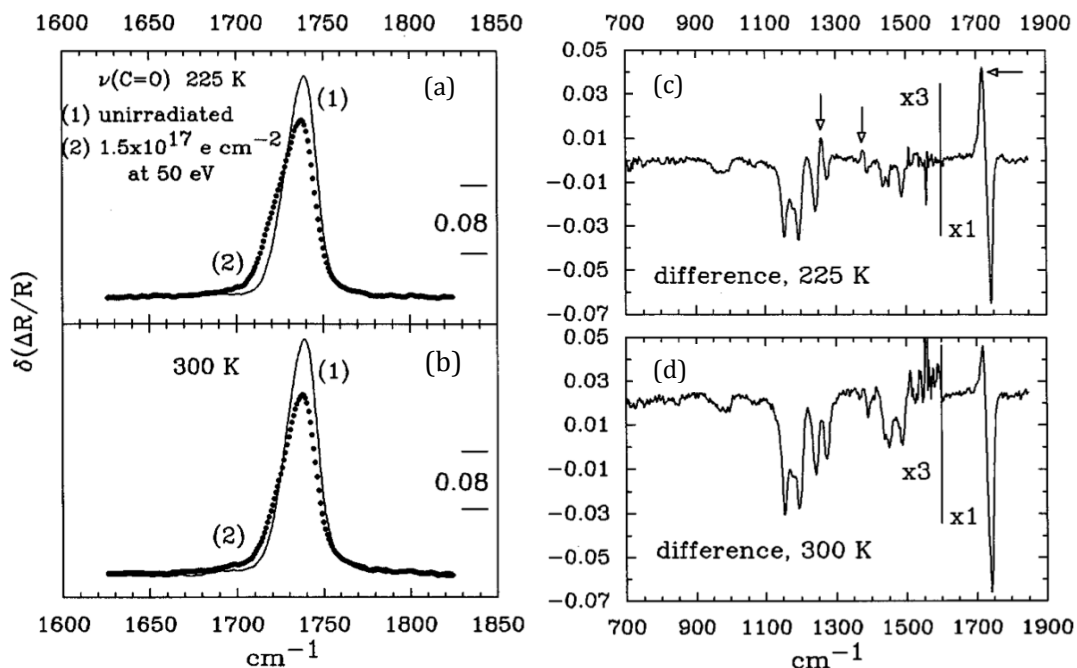


Fig. 12. Effect of a 50 eV electron beam on the $\nu(\text{C}=\text{O})$ band for PMMA/Al at (a) 225 and (b) 300 K and difference spectra at (c) 225 K and (d) 300 K obtained by subtracting the un-irradiated data from 50 eV irradiated data. Note the change of sensitivity scale at 1600 cm^{-1} [4].

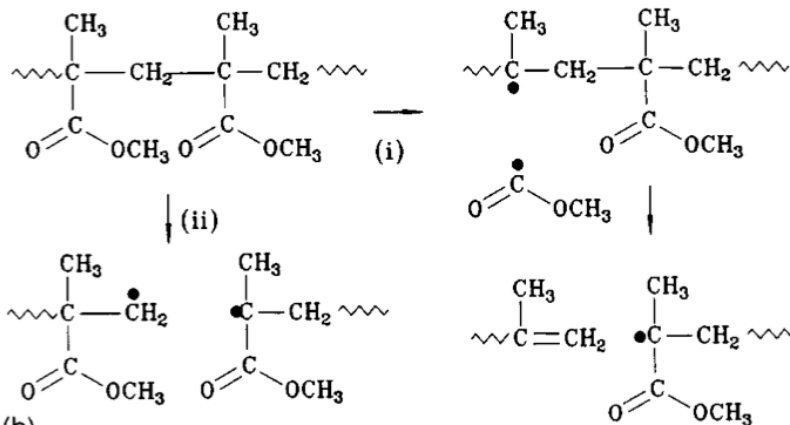
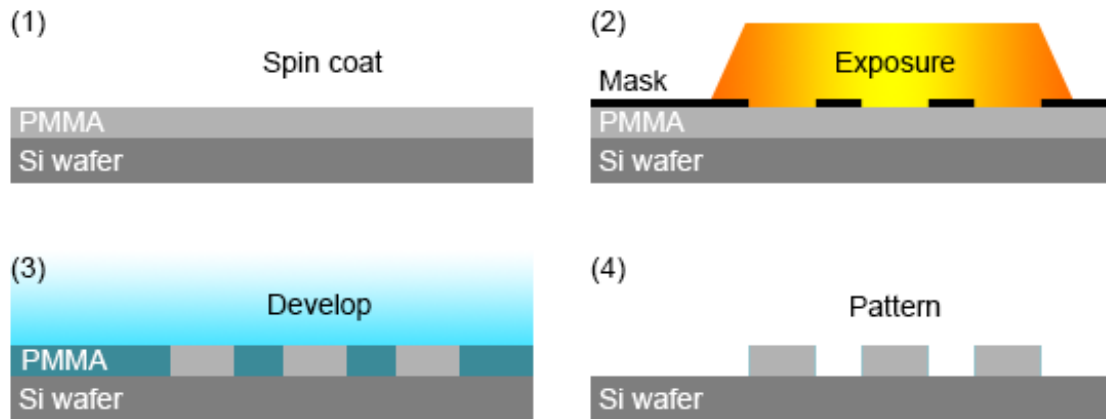


Fig. 13 Proposed electron-induced chain-scission pathways of PMMA. [4]

Main chain scission at the site where the ester group leaves is another possible result from the elimination of the ester group. Two possible pathways are shown in Fig. 13. The first pathway (i) shows the removal of ester group leaves a radical, followed by the formation of $=\text{CH}_2$ end group. The second pathway (ii) is a direct process. The radical species can undergo further reaction of decomposition, releasing CO , CO_2 , etc., or can combine with other radicals.

However, both the fragmentation and chain-scission pathways shown in Fig. 11 and Fig. 13 do not consider the effect of the charge of the electrons. In real situation the radicals can be cations and anions. The mechanism can be different when taking the effect of charge into account.



Negative tone resist PMMA

Fig. 14. A schematic drawing of usage of PMMA as a negative tone resist.

PMMA has a negative tone regime as well. Fig. 14 shows the schematic drawing of PMMA used as a negative resist. Teh et al [9] have studied cross-linked PMMA and use it as a sacrificial layer to fabricate (Nanoelectromechanical systems) NEMS and (Microelectromechanical systems) MEMS suspending structures. They use high voltage electrons (25 keV) emitted from SEM as electron irradiation. The closed symbols in Fig. 15 show the remaining thickness of cross-linked PMMA (molecular weight = 100K) after development normalized to the initial thickness after spin coating as a function of electron dose. The open symbols are from the similar results by Tada et al [10] from the 20K eV irradiation of PMMA with molecular weight of 600K. In both results at a dose range 100 – 7000 $\mu\text{C}/\text{cm}^2$ the PMMA resist is removed after development, as a result of the positive regime of PMMA in lower dose range. When the dose increases from 7000 $\mu\text{C}/\text{cm}^2$ the PMMA molecules cross-link and the resist enters negative regime. Only a fraction of the thin film is removed within this regime until the remaining film thickness reaches maximum of around 55% of the initial spin-on thickness. The PMMA is believed to be fully cross-linked.

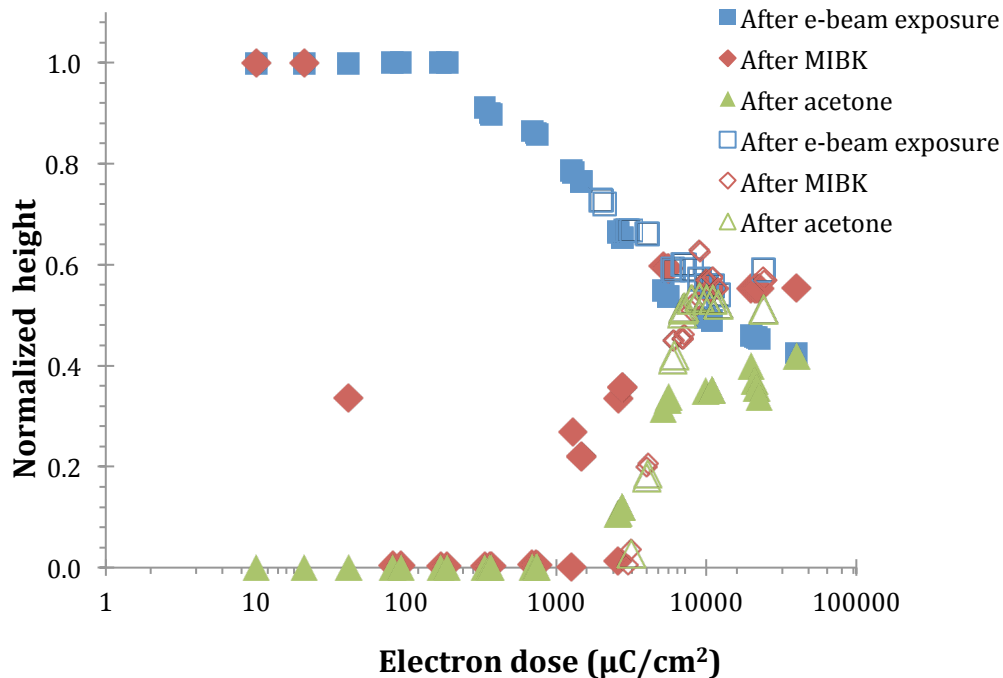


Fig. 15. Thickness of PMMA before and after development normalized by the spin-on thickness as a function of dose. Data reworked from [9](closed symbols) and [10](open symbols).

Lehockey et al [11] proposed a model that describe the decreased solubility of PMMA due to increased molecular weight after certain dose, i.e. the cross-linking process. After the abstracted ester group causes main chain scission, the end radical groups of fragmented PMMA diffuses and are possible reactants for recombination. As the dose increases, the density of the radicals also increases during the competing process of chain scission and cross-linking. The cross-linking finally dominates the competition thus results in the cross-linked PMMA as the final state. Fig. 16 shows the schematic drawing of the end linking of two radical species where subtractions of ester group and chain scissions have occurred. As a result, double bond is formed at the end groups and PMMA is cross-linked.

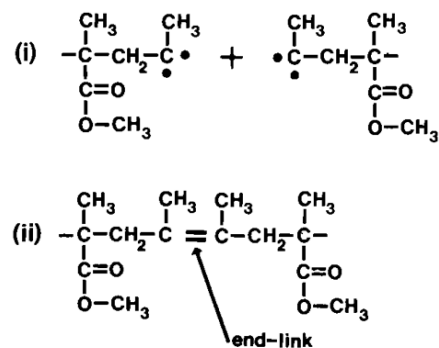


Fig. 16 The proposed mechanism for main chain recombination. [11]

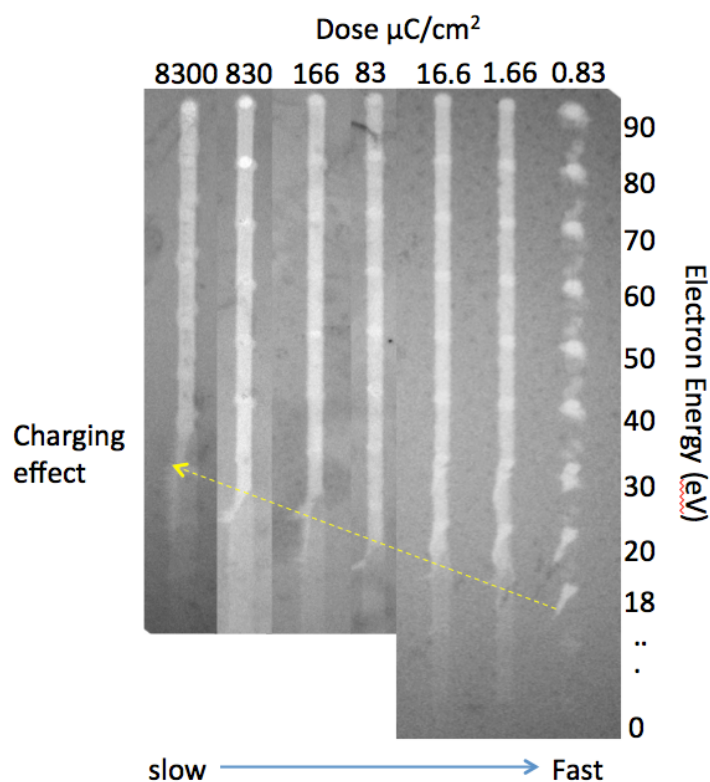


Fig. 17. The charging effect on the threshold of low-energy electron-induced chemistry.

Dr. Aniket Thete and Assoc Prof. S. J. van der Molen in Leiden University studied the energy dependence of low-energy electron-induced chemistry on PMMA using low-energy electron microscopy (LEEM). The zero energy level is first determined by tuning the focus of the condenser optics to a point that the low-energy electrons reflect at the sample surface. The exposure electron energies are given with respect to the zero energy level to irradiate the PMMA samples. Point exposures on a spin-coated PMMA (950K) thin film reveals that there is a threshold around 18 eV for the energy of the electrons exposing the thin film. Above the threshold the exposed areas can be developed, while below the threshold they cannot. They also studied the charging effects of the PMMA on the threshold as shown in Fig. 0. The electron beam is scanning along one lateral direction from bottom to top with energy ranges from 0 eV to 90 eV by moving the sample stage at different speeds. The doses are calculated from the beam currents and the exposed areas. At the fastest scanning speed, which is shown on the right column of Fig. 17, the threshold is around 18 eV. As the speed of scanning decreases, the threshold increases from 18 eV to 30 eV at the given doses. It is because more charge is building up on the surface of the sample during the slower scanning of the beam. This energy threshold will be compared with our results in this thesis in chapter 4.

3. Experimental setup and methods

3.1 Experimental setup

Mass spectroscopy (MS) is used to determine the elemental or isotopic signature of a sample, by acquiring the spectrum of masses of the atoms or molecules. In a typical process the sample is ionized, for instance irradiated with electrons. Some of the molecules break in to charged fragments and are selected according to their mass-to-charge ratio and collected by the ion detector (electron multiplier). In the mass the ion abundance is plotted versus the mass-to-charge ratio, which provides information of the structure of their precursor molecule.

X-ray photoelectron spectroscopy (XPS) is a commonly used chemical analysis technique. XPS uses the photoelectric effect, in which a core level electron is emitted after absorbing a photon with energy higher than the binding energy of the electron. An electron spectrometer will measure the kinetic energy of the ejected electron. The binding energy of the electron can be calculated. The binding energy is the characteristic of the atomic or molecular orbital from which the electron originates. XPS not only enables us to determine the binding energies of electrons, but also provides quantitative information on the chemical composition and the chemical environment of elements (oxidation state, binding to a more or less electronegative element). Changes in binding energies (called chemical shifts), peak areas and peak shapes as result of electron exposures allow us to determine the changes in molecular bindings, reaction rates, etc.

Atomic force microscopy (AFM) is a high-resolution type of a scanning probe microscopy (SPM). A sample is analyzed by probing the surface with a tip, and the interaction between tip and sample is measured. Physical topography can be measured by scanning the tip over the surface of the sample at constant height or constant frequency. In non-contact mode, the tip is driven to oscillate at a constant frequency near its resonance frequency. The height of the tip is changed to maintain the tip at constant amplitude while scanning the surface. The topography of the sample is measured by recording the height of the tip at constant amplitude using a laser.

In our experiment the XPS and MS measurements are done in an ultra-high vacuum system consisting of three customized chambers. The schematic drawing of the system is shown in Fig. 18.

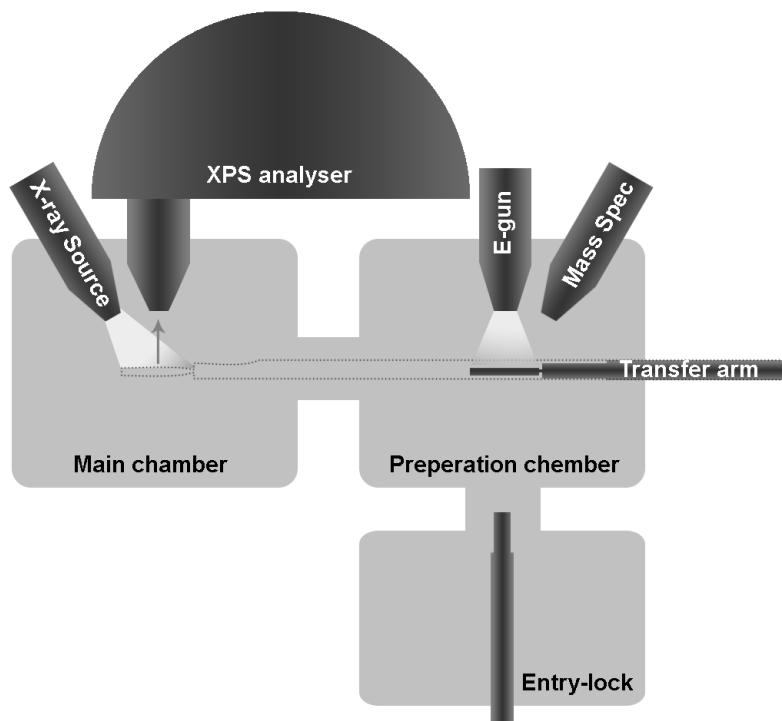


Fig. 18. A schematic drawing of the XPS and MS UHV system.

The main chamber is pumped with an ion getter pump (Varian "Star Cell"), and is equipped with a XPS analyser (VG SCIENTA R3000), monochromic Al $K\alpha$ X-ray source (1486.6 eV) and a flood-gun (SCIENTA Flood-gun 300). The irradiation angle for the incoming X-ray is 54 degrees and the detector is perpendicular to the sample surface. The spot size of the X-ray is about 3 mm by 1mm. The flood-gun for charge compensation has a tunable energy range of 0 – 10 eV.

The preparation chamber is pumped by a turbo-molecular pump (PFEIFER TMU-521P) backed with a membrane pump (Membran Vacuubrand MD4), and is equipped with a tunable flood electron gun (1 eV – 2000 eV, Kimball Physic ELG-2), a quadruple mass spectrometer (MKS "VAC-CHECK"), a faraday cup, and a xyz manipulator. The flood gun has a two-dimensional deflection function and is programmed with a line-by-line scanning function to achieve a relative uniform large area surface exposure. The faraday cup with current-limiting aperture of 2 mm in diameter can be placed directly beneath the electron gun to measure the current.

The manipulator has a metal sample holder with two metal clamps to hold the sample and ground it. Using the manipulator the sample can be transferred for XPS measurements, electron irradiation and sample import/export.

The entry-lock is used to load/unload the sample, and is pumped by a turbo-molecular pump and a membrane pump (Membran Vacuubrand MD4).

All the chambers can be separated with valves and were separated during the measurements, except for during the XPS measurements when the manipulator is preventing the separation between main chamber and preparation chamber. The pressure readings in the chambers are measured using ion-gauges separately. All the measurements are conducted at a base pressure below 3.0×10^{-9} mbar. All the exposures are conducted at a base pressure below 3.0×10^{-8} mbar.

3.2 Materials used

The PMMA solution used in all experiments is purchased from ALLRESIST, type ARP-631.09. It has a molecular weight of 50K and solid content percentage of 9%, and is dissolved in chlorobenzene. The toluene (99.5%) used to dilute the PMMA solution in all experiments is purchased from Analytical Reagent A.R. The developer solution are prepared by mixing the MIBK (methyl isobutyl ketone):IPA (isopropyl alcohol) = 1:3. The MIBK (99.5%) is purchased from Acros Organics, and the IPA (99.7%) is purchased from Analytical Reagent A.R. The acetone (99.5%) used for cleaning the silicon wafers is purchased from Analytical Reagent. A.R.

3.3 Preparation of PMMA thin films

The thin films of PMMA resists are spin-coated on silicon wafers pieces cut to dimension of 9.0 x 11.0 mm. Christopher et al find that the thickness and uniformity of the PMMA thin films coated by PMMA with a solution of toluene are superior to solutions of chloroform [12]. They attribute this to the slower evaporation speed of the toluene after coating and longer time that is available for film formation before the solvent evaporates. As shown in Fig. 19, the spin-coated film thickness is inversely proportional to the polymer concentration of the solution [13], and toluene is miscible with chlorobenzene and chloroform, we use toluene to dilute the original solution of PMMA.

PMMA solution is prepared by diluting the as-received solution with toluene. The chlorobenzene solution of PMMA and the toluene are mixed with a volume ratio of 1:4, producing a 5 times diluted solution of PMMA. Because the surface sensitivity of XPS is around 10 nm and there will be charging on the surface of PMMA films, we want to make the PMMA films as thin as possible.

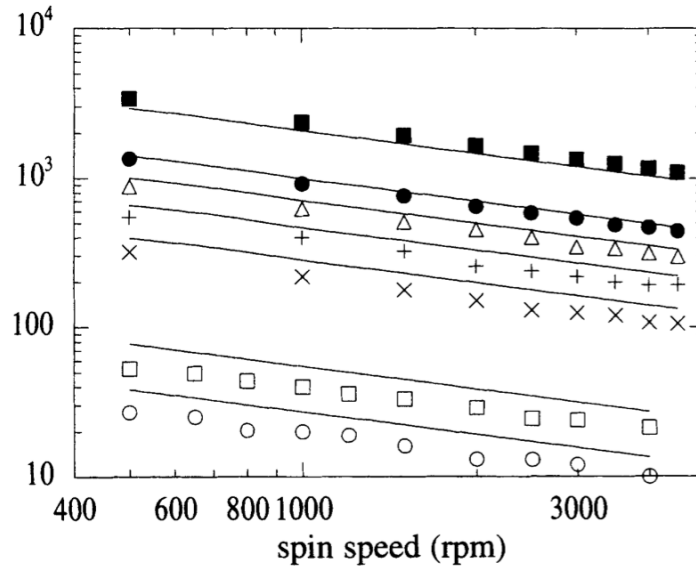


Fig. 19. PMMA film thickness as a function of spin speed from different initial PMMA solution concentrations in toluene. [13]

Before spin coating the silicon wafers are washed three times with acetone and IPA, and dried with nitrogen. We choose a spin speed of 10000 rpm to coat the thin film for 60 seconds. As a result, the film spun using these parameters has a uniform color dispersion around the center if examined by eye, and the corners and edges of the film are a bit darker because of the surface tension of the solution during spinning. After coating we bake the sample at 180 °C for 2 minutes for curing. After that the darker features around the corners and edges disappear, indicating that a uniform surface is achieved. The samples prepared after baking are directly exposed or measured by XPS without further treatment.

3.4 Low-energy electron irradiation

Before exposing the sample, the current density of the emitted electron beam is measured using the Faraday cup. The Faraday cup is aligned to the position where the electron gun is right above the current-limiting aperture. The electron gun is aligned until the focused beam enters the Faraday cup and the current reading reaches the maximum on the ammeter. The typical current reading of the Faraday cup is around 1620 nA for a stationary electron beam. When the scanning function of the electron gun is switched on, the current density is measured and the uniformity of the area exposure is checked, i.e. the current density exposing the edge of the sample does not drop below 80% of the central density. The scanning beam area is about 1.2 cm × 1.2 cm, and covers the sample. The typical current reading of the Faraday cup during scanning is around 140A, corresponding to a current density of around 44.6 $\mu\text{A}/\text{cm}^2$. In our experiments we used the electron gun with an energy range 5 – 40 eV.

To expose the PMMA thin films with electrons, the samples are introduced into the UHV system and moved to the position around 2.5 cm under the electron gun. The electron gun is positioned right above the sample at an angle of 90°. The electron gun is set to the saved setting and the grid voltage is set to a high value to blank the beam. The sample holder is grounded so that the electrons emitted from the electron gun have the preset landing energy if there is no charging on the surface.

The mass spectrometer is switched on with a fast scan function before exposure and the background pressure of selected masses is recorded for around five minutes. The sample is exposed by setting the grid voltage to 0 V. Typical total pressure readings on the ion gauge in the preparation chamber goes as high as 2.5×10^{-8} mbar after the irradiation starts. The mass spectrometer records the out-gassing pressures caused by electron irradiation during the exposure. The scanning rate is around 0.9 scans per second for all the selected masses. In our case the selected masses are 2, 15, 28, 31, and 44. Setting the grid voltage back to high value stops the exposure. The mass spectrometer continues to record the background level for another five minutes.

The exposed samples are used for characterization or development without further treatment.

3.5 Development

The exposed samples are developed with a developer MIBK:IPA = 1:3. To develop the samples, the samples are dipped into the developer for one minute, and then dipped into pure IPA for another minute. The cycle is repeated for 3 times before the samples are dried with nitrogen.

3.6 AFM measurement

The film thickness after exposure is measured by an AFM (BRUKER MultiMode® 8) equipped with a tapping-mode silicon tip (Tap300 from Budgetsensors) with a resonant frequency of 300 kHz and a force constant of 40 N/m, running at tapping mode for samples before and after development. In order to get a step profile from the thin film, the samples are scratched with a clean wood stick to remove several lines of PMMA. The AFM images of the edges of the step features are taken and analyzed to calculate the thickness of the films. After development the same scratches are measured in comparison with the thickness before development.

4. Results and discussions

4.1 Threshold energy of exposure

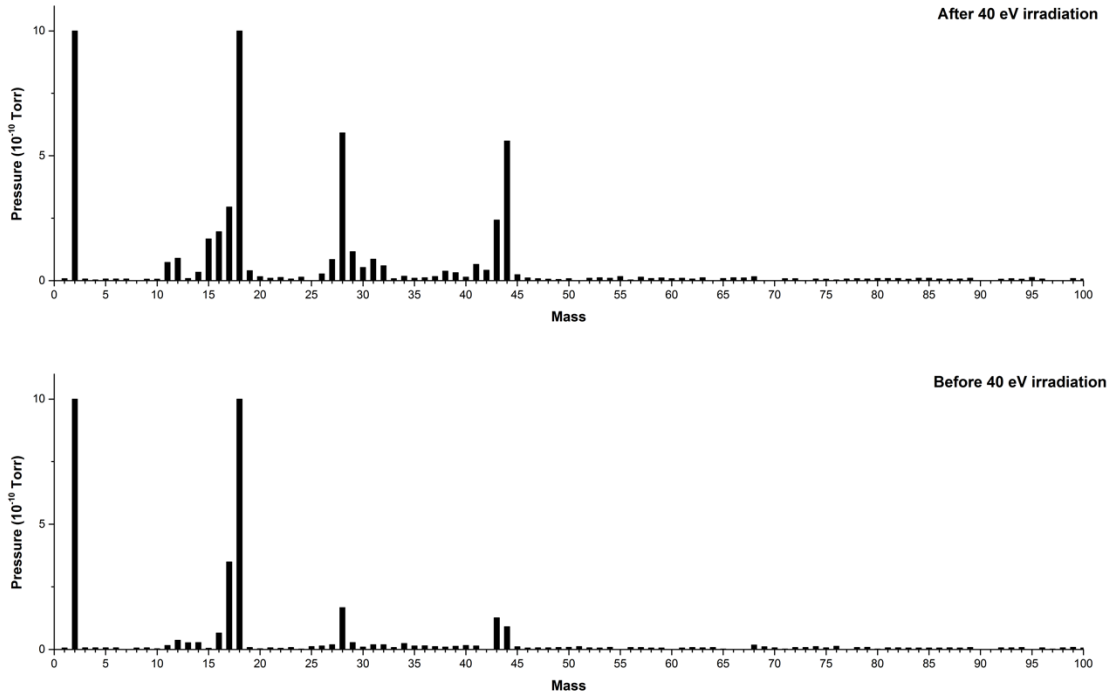


Fig. 20. Mass spectra of mass 1 to 100 from PMMA before and after irradiated with 40 eV electrons.

Mass spectra during exposure of 40 eV electrons before and after irradiation are recorded. The results are shown in Fig. 20. In mass scans from $m = 1$ to $m = 100$, gas fragments of mass 2, 15, 28, 31 and 44 show an increase from the background level when the irradiation is switched on. As the irradiation continues, the pressures of the previously mentioned masses decay with time except for mass 2 (H_2 molecules). The origin of high amount of hydrogen desorption is explained by Hiraoka as a result of the production of negative hydrogen ions by low-energy electrons [14]. When the irradiation is switched off, the partial pressures of the selected masses reach the background again.

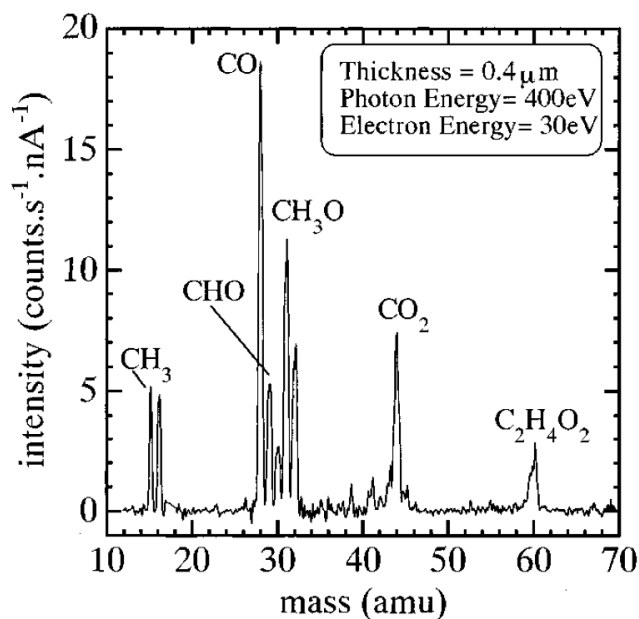


Fig. 21 Mass spectrum of a thin film of PMMA using 400 eV synchrotron irradiation and 30 eV electron energy of the ionizer. The peaks were assigned to neutral photo-desorption products. [15]

The molecular fragments can be assigned to fragments of PMMA that are produced during irradiation. Mass 15 corresponds to a methyl group ($-\text{CH}_3$) from the side chain of PMMA. Mass 28 corresponds to a carbonyl group ($-\text{C}=\text{O}$) in the side chain. Mass 31 can be assigned to a methoxy group ($-\text{O}-\text{CH}_3$). Mass 44 can either be carbon dioxide molecule or a carboxylate group ($\text{O}-\text{C}=\text{O}$). Similar results of degassing are found by Tinone et al [15]. Fig. 21 shows the mass spectrum of PMMA exposed by 400 eV soft X-ray. Both results confirm the dissociation mechanism proposed in Fig. 11 as mentioned in Chapter 2. The molecular fragments are results of dissociation of the subtracted ester group. There are two possible pathways, one forming $-\text{CH}_3$ and $\text{O}-\text{C}=\text{O}$ while the other forming $-\text{O}-\text{CH}_3$ and $-\text{C}=\text{O}$.

A difference between our results in Fig. 20 and those obtained by Tinone et al is that, in our results the peaks of mass 59 and 60 (ester group) are not visible in the mass spectrum during irradiation, while they observe those masses with high yields. The possible origin of this deviation is that we use different irradiation energy (40 eV) and a different type of irradiation (low-energy electrons other than 400 eV soft X-ray). The low sensitivity of our quadrupole mass spectrometer can also explain the absence of mass 59 and 60.

To investigate the energy dependence of the reaction of PMMA induced by low-energy electrons, we exposed samples with electron energies ranging from 5 eV to 40 eV for around 20 min with a scanning beam at current density around $4 \mu\text{A}/\text{cm}^2$. Mass spectra

of the samples are taken during the irradiation and we trace the masses 2, 15, 28, 31, and 44. Each fast scan of the masses from different energies is shifted so that the pressure plateau at dose 2500 $\mu\text{C}/\text{cm}^2$ is 0 mbar to exclude the background. The pressure at lower dose indicates the partial pressure that is induced by the irradiation.

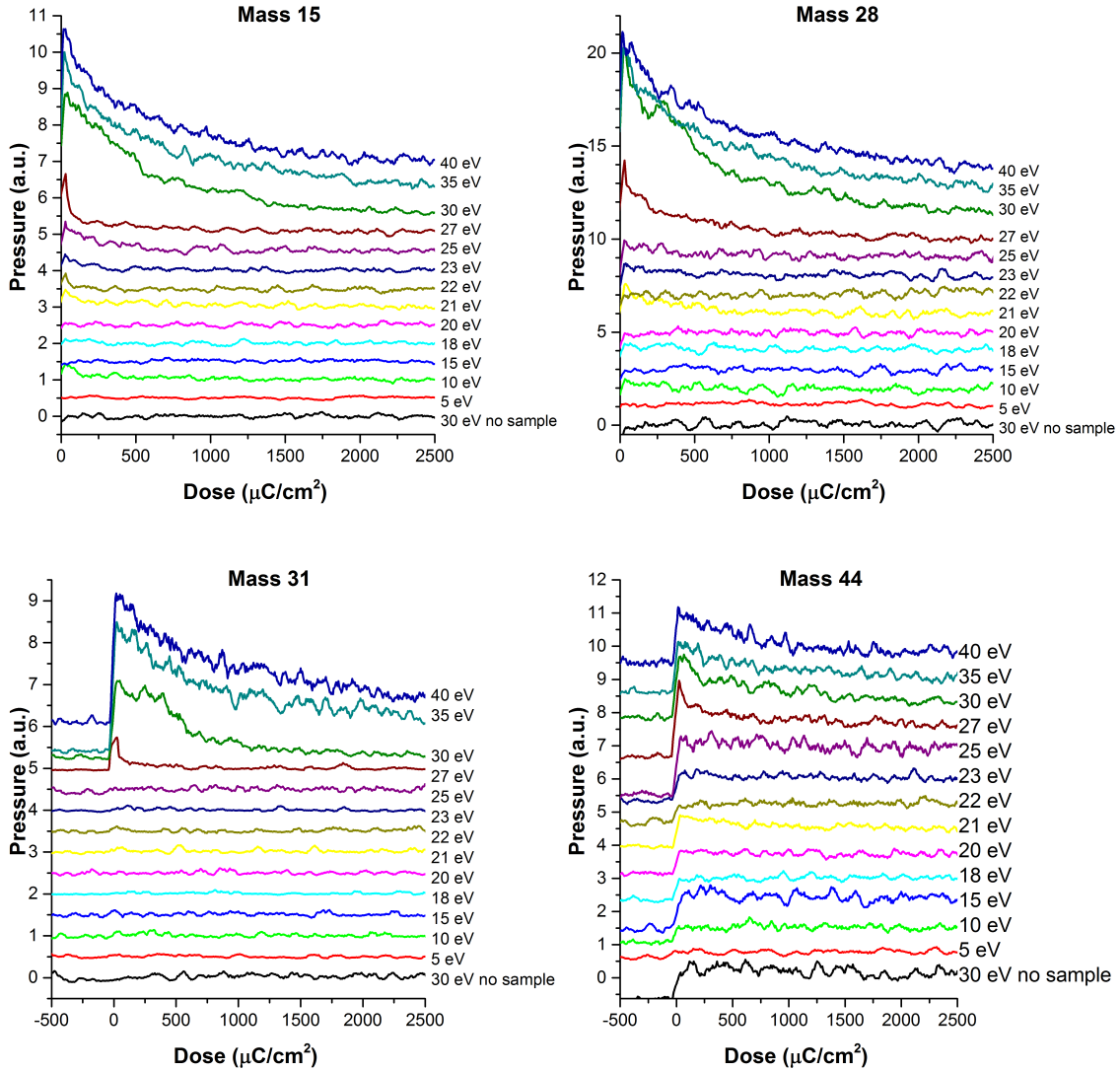


Fig. 22. Fast scan mass spectra of mass 15, 28, 31 and 44 from PMMA irradiated with electrons with energy range from 5 eV to 40 eV.

Fig. 22 shows the fast scans of the partial pressure of mass 15, 28, 31, and 44 during the irradiation of electrons with energy 5 – 40 eV as a function of dose. It is observed that for higher energy irradiations, for example in the 35 eV and 40 eV spectra of mass 15, the degassing of PMMA drops with dose. Sharp increases after the irradiations are switched on can be found for these spectra. For lower energy irradiations, for example the 15 eV spectra of mass 44, a step increase is also found. However the step jump

does not decay as the dose increases. Mass spectra of irradiation of the sample holder without the sample are acquired. It is shown that the step increases also occur in mass 15, 28 and 44. These step increases are believed to be caused by electron-induced desorption of absorbed background gases in the equipment, such as CO (28), CO₂ (44) H₂O (18). We will discard these step increases and distinguish them from the sharp increase caused by degassing from the sample.

Amongst all spectra the sharp increases after switching on the irradiation occur only above certain energies, none of them occurs for electron energy below 20 eV for all masses, except for the mass 15 spectra there's a small jump for 10 eV electrons irradiation. The threshold energy sits at similar value (around 27 eV) for mass 31 and mass 44. Below 27 eV there's no significant step jump at the beginning of irradiation. For mass 15 the threshold appears around 21 eV while for mass 28 the threshold is around 23 eV. For mass 44 the signal-to-noise ratio is too low to record the slight increase in pressure below 27 eV. However, mass spectra from mass 31 have the lowest background noise thus it gives the most convincing result. These thresholds are believed to be higher than the real threshold because of the charging induced by the electron irradiation during the exposure. We will discuss this later in a separate chapter.

In the mass 15 spectra a small jump is also found for 10 eV electrons irradiation. This is below the threshold we proposed. Similar phenomenon is also found for 21 eV electrons irradiation in the spectra of mass 28. Because these electron energies are below the energy onsets obtained by our results, they seem to have the characteristic of resonance scattering as described in Fig. 5. However the energy of the electron is too high to be attributed to the DEA resonance. The 10 eV jump in the spectrum of mass 15 is more likely to be an artifact.

4.2 Decomposition of PMMA

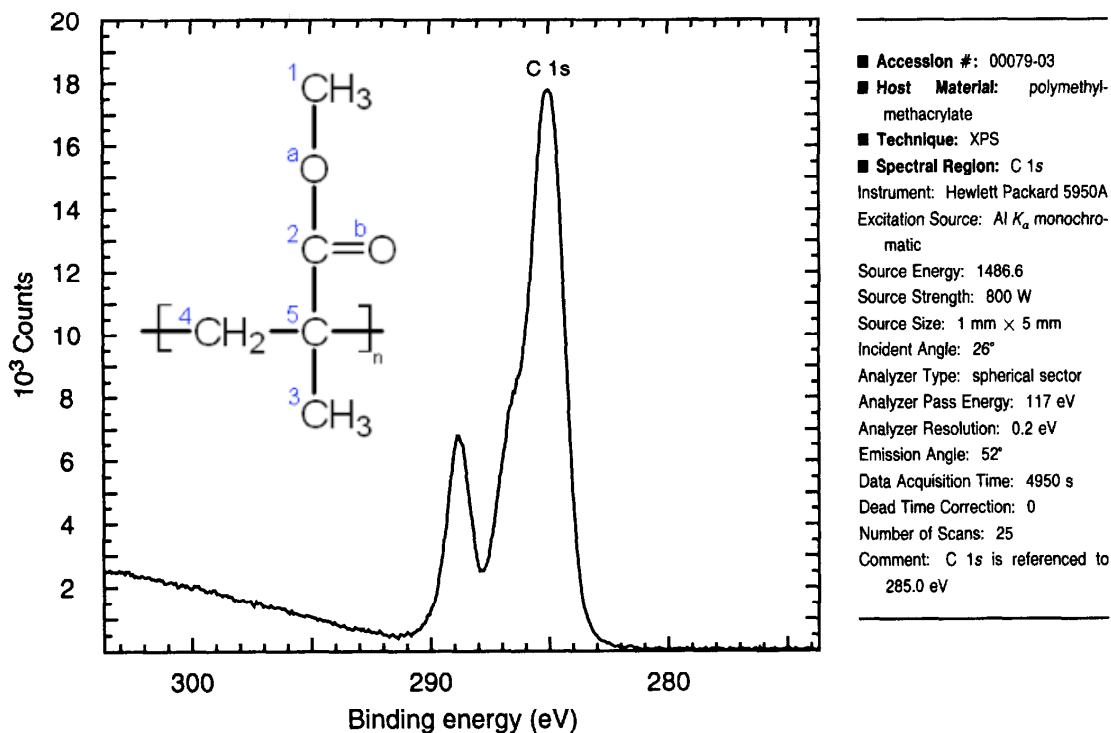


Fig. 23. A typical XPS spectrum of carbon 1s in PMMA.[16]

A typical carbon 1s spectrum of PMMA is shown in Fig. 23. The carbon 1s spectrum of PMMA is deconvoluted using Gaussian functions in Fig. 24. The components can be assigned to carbon atoms in four oxidation states in the repeating units of PMMA. Gross et al fit the spectrum with a 1:1:1:2 peak fitting scheme [17], which gives an accurate fitting of PMMA. The component with the largest intensity is at 286.2 eV, corresponding to the carbon atom with the lowest electronegativity, i.e. the carbon atoms of the bone structure of the polymer (C4 & C5). The shoulder of this component lays around 286.8 eV and can be fitted with a Gaussian, corresponding to the carbon (C3) with higher electronegativity, the methyl group attaching to the bone structure. The components at 287.8 eV and 290.1 eV can be assigned to the double-bonded (C2) and single-bonded (C1) carbon, respectively. The areas of the fitted components reflect the atomic distribution of the carbons with different chemical environment. The ratio of the areas is in well agreements with the number of the carbon atoms in the structure. The spectrum is shifted in energy compared to the reference spectrum in Fig. 23 as a result of charging on the sample. It will be discussed later in a separate chapter.

The oxygen 1s spectrum of PMMA can be deconvoluted using Gaussian functions as well (deconvolution of the spectrum not shown here). The deconvolution results in two components: one at higher binding energy corresponds to the single-bonded oxygen

(Oa); the other one at lower binding energy corresponds to the double-bonded oxygen (Ob). Two components have similar areas whereas the Oa component has a slightly lower intensity.

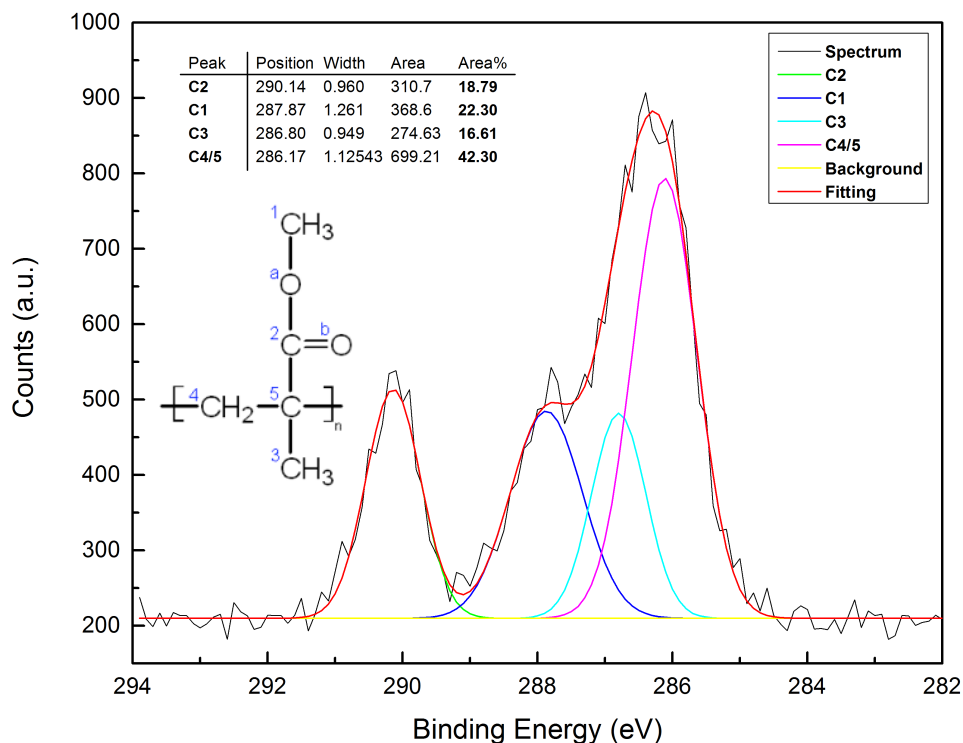


Fig. 24. A deconvolution of the unexposed PMMA with Gaussian functions.

To study the dose dependence of the dissociation of the PMMA molecule, we take XPS spectra of carbon 1s and oxygen 1s of PMMA during irradiation using different doses. Fig. 25 (a) shows the carbon 1s spectra of a PMMA sample irradiated with 20 eV electrons at several doses. At $0 \mu\text{C}/\text{cm}^2$ the spectrum is in agreement with the reference data. As the dose increases the peaks shift as a whole to lower binding energy and the peaks become broader. The two components belonging to C1 and C2 decrease in intensity and area. At a dose higher than $2316.2 \mu\text{C}/\text{cm}^2$, the spectrum starts to shift back to higher energy. At a dose of around $23166.0 \mu\text{C}/\text{cm}^2$ the peaks of C1 and C2 disappear completely, and the shoulder of the largest peak (C4/5) disappears that makes the peak almost symmetric. The intensity of the component C4/5 increases around 15% with respect to the original peak intensity. The center of the largest component ends at a binding energy around 285.3 eV, which is very close to its reference data (285.0 eV). Fig. 25 (b) shows the oxygen 1s spectra of a PMMA sample irradiated with 20 eV electrons at several doses. At $0 \mu\text{C}/\text{cm}^2$ the spectrum consists of two components at 534.8 eV and 533.3 eV. As the dose increases the component associated with single-bonded oxygen (Oa) disappears while the double-bonded oxygen remains unchanged. The spectra of oxygen also shift as a whole as dose change, similar

as we see for carbon spectra. However the amounts of shift are slightly different for carbon and oxygen spectra.

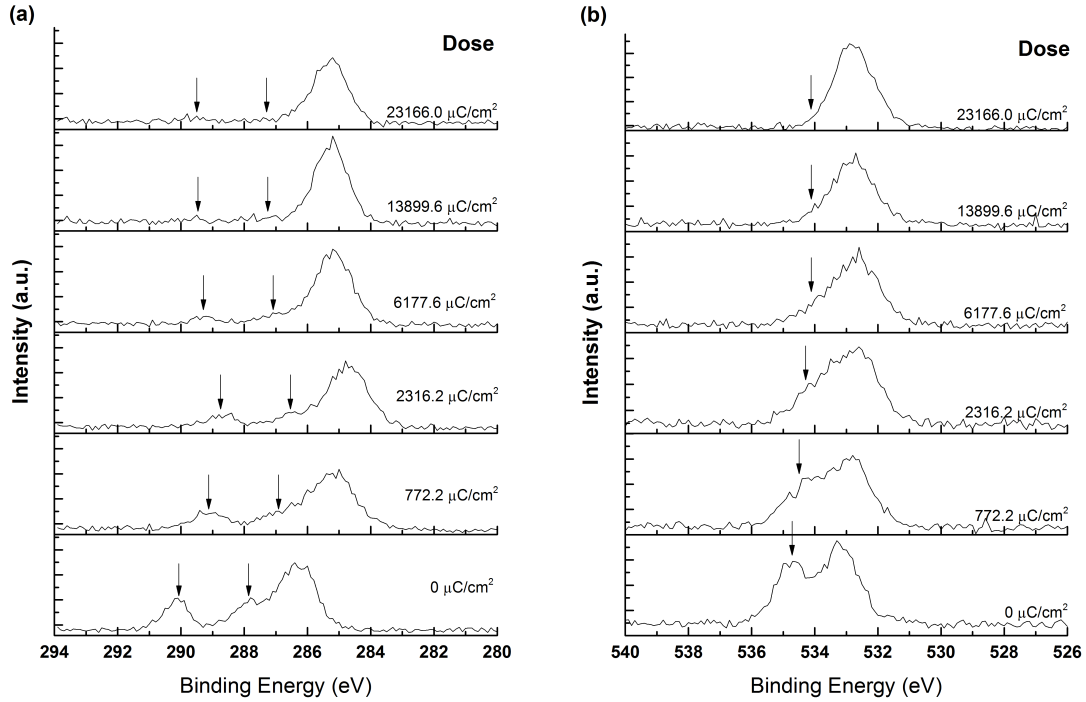


Fig. 25. Spectra of (a) C 1s and (b) O 1s of PMMA with increasing doses of irradiation by 20 eV electrons.

Detailed quantitative analysis of the peak areas can be achieved by fitting of the spectra with the same component separations and similar ratio between the component widths as the reference data. By doing this, the chemical shifts of individual components are neglected because it is difficult to distinguish between the shifts due to chemical changes and the shifts due to charging. The areas of the individual peaks are calculated through fitting and normalized with the relative sensitive factor of the elements. Both carbon and oxygen peaks are analyzed and normalized so their peak areas can be compared. Fig. 26 shows the area of the peaks of both carbon and oxygen as a function of dose.

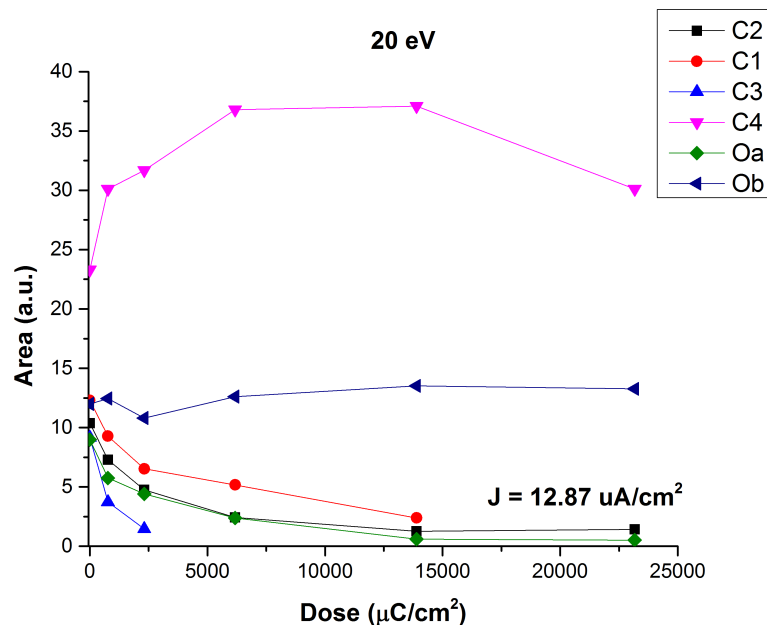


Fig. 26. Relative peak areas as a function of dose.

A rapid increase of peak C4 can be found at dose from 0 to 2500 $\mu\text{C}/\text{cm}^2$, after which a plateau is shown and at higher dose it starts to decrease. The area of peak Ob remains the same through out the irradiation process. Other peaks of carbon and oxygen decays as increasing dose and reaches 0 at certain doses. The decreasing of peak areas indicates that the chemical environments of corresponding carbons are changing as bonds are breaking. The curve of C2 and Oa almost overlap, indicating a possible correlation between these two atoms. The decrease speed of C3 appears to be higher than that of C1. It could suggest that the reaction speeds the two methyl groups are different, but cautions should be given before drawing this conclusion since the fitting of the large component and its shoulder can introduce a large error. The increase in area of component C4 as the dose increases at doses 0 $\mu\text{C}/\text{cm}^2$ to around 14000 $\mu\text{C}/\text{cm}^2$ suggests that one or more carbon atoms from C1, C2 and C3 are reacting to yield carbon atoms with similar oxidation state as C4.

The correlation of the two components suggests that the reaction happens between C2 and Oa, i.e. the dissociation occurs between C2 and Oa. This result fits well with one of the dissociation mechanism of the ester group that leads to molecular fragments of $-\text{C}=\text{O}$ and $-\text{O}-\text{CH}_3$. However, the XPS spectra of oxygen suggest that only one of these two fragments is leaving the sample, i.e. only $-\text{O}-\text{CH}_3$ group is leaving. The area of the double-bonded oxygen does not change much during the irradiation. Comparing this result to the mass spectra of mass 28, it can be suggested that the out-gassing of mass 28 (CO) does not originate from the double-bonded oxygen. One possible origin is the dehydration from the fragment $-\text{O}-\text{CH}_3$. The fragments with double-bonded oxygen are believed to have remained in the film, for example they are trapped in the PMMA film.

However no carbon counterpart with an oxidation state that is doubly bonded to this oxygen is found to remain. Possible explanation is that the double-bonded oxygen is trapped in the film as CO and CO₂.

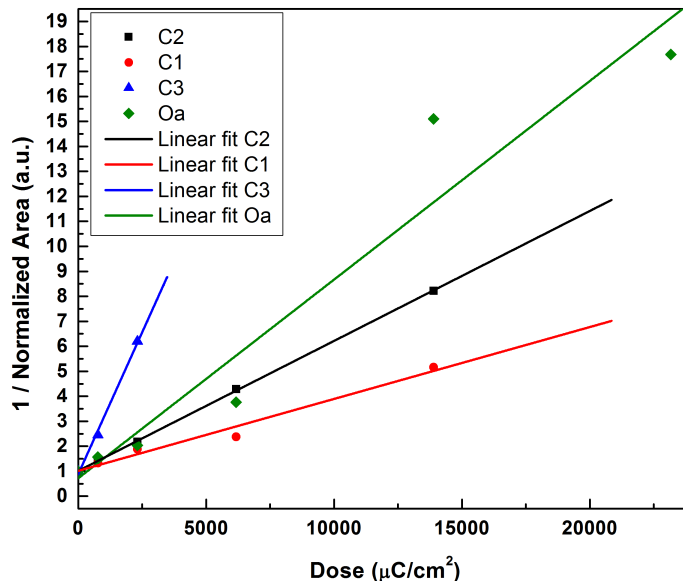


Fig. 27. Linear fits of the reciprocal of the normalized component areas as a function of dose.

In Fig. 27, the areas of the components corresponding to C1, C2, C3 and Oa are normalized by their unexposed values respectively and are plotted reciprocally as a function of dose. Linear fits of each component can be achieved, indicating that the reactions associated to these components are second-order with respect to the electron dose according to the integration of the second-order law:

$$-\frac{1}{[A]} = \frac{1}{[A]_0} + kt$$

However, the reaction rates derived from the linear fittings differ between components. This difference is possibly induced by the system error when deconvoluting the overlapping components using fixed peak separations. The degassing can also lead to different reaction rates. During the fragmentation process different fragments are either released from or trapped in the films. The released fragments are pumped out with different pumping speeds. We cannot determine whether these differences of reaction rates are real or not. But the second-order fittings clearly indicate that the low-energy electron-induced reactions that cause the dissociations of these components are two-step. This result fits well with the two-step dissociation mechanism proposed in chapter 2.2.

Similar experiments are done with 10 eV and 30 eV electrons as well. Note the doses used in these experiments are lower than those used in 20 eV exposure. Fig. 28 shows the differential areas of the components during the irradiation of 10 eV and 30 eV electrons. The differential areas are calculated by subtracting the fitted component areas during irradiation by the fitted original component areas before irradiation.

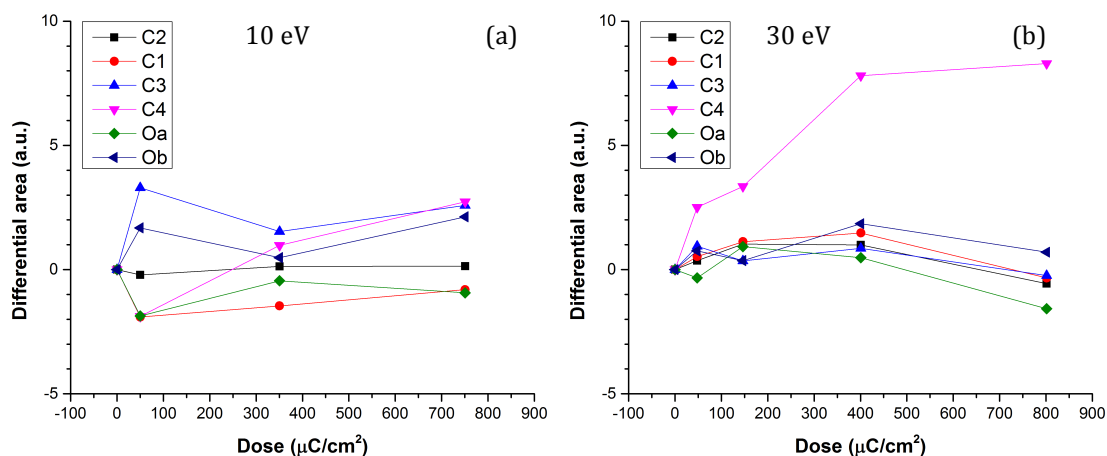


Fig. 28. Difference areas as a function of dose during the irradiation of PMMA with (a) 10 eV electrons and (b) 30 eV electrons. The difference areas are calculated by subtracting the fitted component areas during irradiation by the fitted original component areas before irradiation.

In Fig. 28 (a) the differential areas of the components show some fluctuations around the zero level. We believe these fluctuations are caused only by the errors introduced in the deconvolutions of the spectra. That is, the areas of the components in XPS spectra do not vary much for 10 eV exposures. While in Fig. 28 (b) the differential areas are changing. The component area of C4 is increasing as the dose increases. The areas of other components start to decrease at doses around $400 \mu\text{C}/\text{cm}^2$ after being steady from doses from 0 to $400 \mu\text{C}/\text{cm}^2$. This confirms that the threshold energy of the electron-induced reaction is between 10 eV and 30 eV.

MS measurements suggest that the reactions are already complete to a large extent at dose $500 \mu\text{C}/\text{cm}^2$, while in XPS measurements the areas of the components do not decrease as the dose increases at doses 0 to $400 \mu\text{C}/\text{cm}^2$, except for the area of C4, which is increasing. This is probably caused by the difference in continuous exposure and alternating X-ray and electron exposure. When the sample is irradiated with X-ray, the electrons exposed to the sample will neutralize the charge before reach the reaction sites.

4.3 Crosslinking of PMMA

Two groups of samples with different dose of exposure by 10 eV and 30 eV electrons are prepared to study the dependence of film thicknesses on irradiation energy and dose. Several scratches are put on each sample by a wood stick thus remove the scratched PMMA after irradiation. AFM images of the areas of the scratches are taken for all the samples before and after development with the developer (MIBK:IPA = 1:3). The thicknesses of the films before and after development are measured by analyzing the average differences of the thicknesses between scratched and un-scratched areas. Fig. 29 shows the dependence of film thickness on dose for samples exposed by 10 eV and 30 eV electrons.

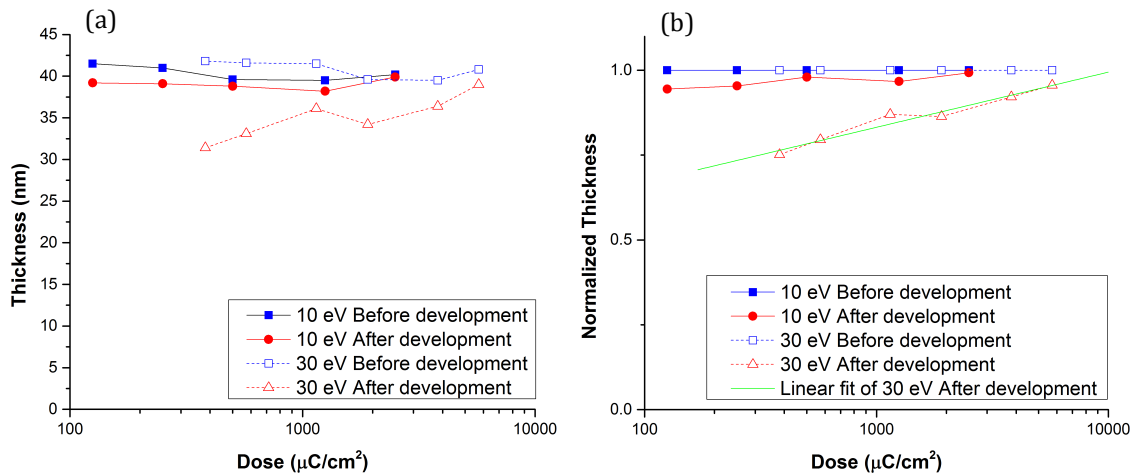


Fig. 29. (a) The film thicknesses of PMMA before and after development as a function of dose for samples exposed by 10 eV and 30 eV electrons. (b) Normalized film thicknesses by un-exposed thicknesses.

As shown in Fig. 29 (a), the film thicknesses of un-developed samples are approximately the same for both 10 eV and 30 eV exposures. There's a slight decrease of thickness after the sample is exposed to specific dose. For 10 eV exposures the decrease happens around $500 \mu\text{C}/\text{cm}^2$, and for 30 eV exposures the decrease happens around $1000 \mu\text{C}/\text{cm}^2$. After development, the film thicknesses of the 10-eV-exposed samples remain the same; only an insignificant decrease is found around 1 – 3 nm. While for the 30-eV-exposed samples the decrease in thickness is clear. For example at a dose of $380 \mu\text{C}/\text{cm}^2$, the film thickness of the same sample after development is 10.4 nm thinner. The difference in film thickness before and after development decreases as the dose increases, as a result of the decrease of solubility of PMMA in the developer. This implies that the PMMA is crosslinking, from a dose lower than $380 \mu\text{C}/\text{cm}^2$, which is the first data point we measured for 30 eV exposures. For 10 eV exposures, the samples are not developed. Thus 10 eV electrons induce none or little chemistry, confirming that the energy threshold for the chain scission of PMMA is between 10 eV and 30 eV.

The film thicknesses after development are normalized by the thicknesses before development from the same samples individually. The results are plotted in Fig. 29 (b). The decrease in thickness for 30 eV exposures can be fit by a linear function. The dose when the film is fully cross-linked can be extrapolated by the denotation of the linear fitting. The value is around $10000 \mu\text{C}/\text{cm}^2$. Comparing this result with the results shown in Fig. 15, the fully cross-linked dose of 30 eV electron exposures sits around the same value as it of 25 keV electron exposures. This allows us to calculate the efficiency of the generation of secondary electrons from 25 keV high-energy electron irradiations. The secondary generation efficiency is around 1. Therefore, there is one secondary electron in average with energy above the energy threshold for PMMA chain scission that can be generated for each 25 keV high-energy primary electron.

4.4 Charging of PMMA

PMMA is an insulator. The charging on the PMMA thin films are causing various problems throughout the study. The charging of the PMMA is believed to result by two main mechanisms: the positive charge induced by the XPS measurements and the negative charge induced by the electron irradiation. The electron gun induces the negative charge directly by the irradiating electrons, while the X-ray that is generating the photoelectrons induces the positive charge because electrons are leaving.

As Fig. 25 shows the whole spectra of either carbon or oxygen is shifting during the XPS measurements. At lower doses, the spectrum shifts to higher binding energy with respect to the reference spectrum shown in Fig. 23. At higher doses, the spectrum shifts back to lower binding energy and approaches the reference value. Two mechanisms that induce charging are occurring at the same time since the XPS measurements are done immediately after each irradiation of the same sample. At lower doses, the irradiation induced negative charge is not large enough to compensate the X-ray induced positive charge. We believe that the film is positively charged during the irradiation at lower doses. The positively charged film will reduce the kinetic energy of the emitted photoelectrons, thus increase the binding energy calculated. As the dose increases to the specific dose, the irradiation induced negative charge is just enough to compensate the positive charge induced by the X-ray. The resulted spectrum will give the correct binding energies. At higher doses, the film is negatively charged during the XPS measurements. The measured binding energies become lower than the real values.

Individual spectra in many of the XPS iterations are also found to shift during the measurements (data not shown here). The X-ray induced positive charge is compensating the negative charge on the sample in every iteration. Obviously, it will result in peak broadening because the iterations are added up to increase the signal-to-noise ratio. Indeed, the peak broadening is found in our results as shown in Fig. 25. The broadened peaks will bring difficulties in deconvoluting the peaks thus increase fitting errors. Lateral differential charging also causes peak broadening; different charged areas on the sample surface will give different binding energies for same component. The clamps that fix the sample on the sample holder also cause the partial transportation of the electrons from sample surface to ground, causing lateral differential charging.

Another problem caused by charging is that the landing energy of the low-energy electrons becomes hard to predict. Once the electrons reach the surface of the sample, charge starts to build up on the sample surface and slows down the electrons that are approaching the surface. The real landing energy of the electrons is in fact smaller than the emitted electrons from electron gun. This makes the thresholds we seen from mass

spectra higher than real values. As a result of this, the threshold seen in our MS measurements are 3 – 9 eV higher than those results from LEEM.

The XPS spectra of 20 eV exposures show that the reaction is happening for 20 eV exposures, which is below our threshold value found by mass spectra. It is not a contradictory result but may be a result of the alternating irradiations of X-ray and electrons during XPS measurements. The samples become negatively charged after exposure with electrons. Possibly, the charge has been compensated/overcompensated after XPS measurements. The electrons reaching the sample surface now have the correct energies, or even higher energies because the positively charged sample surface. This indicates that the real energy threshold for dissociation of PMMA is around 20 eV, which is consistent with the threshold around 18 eV measured by Aniket et al.

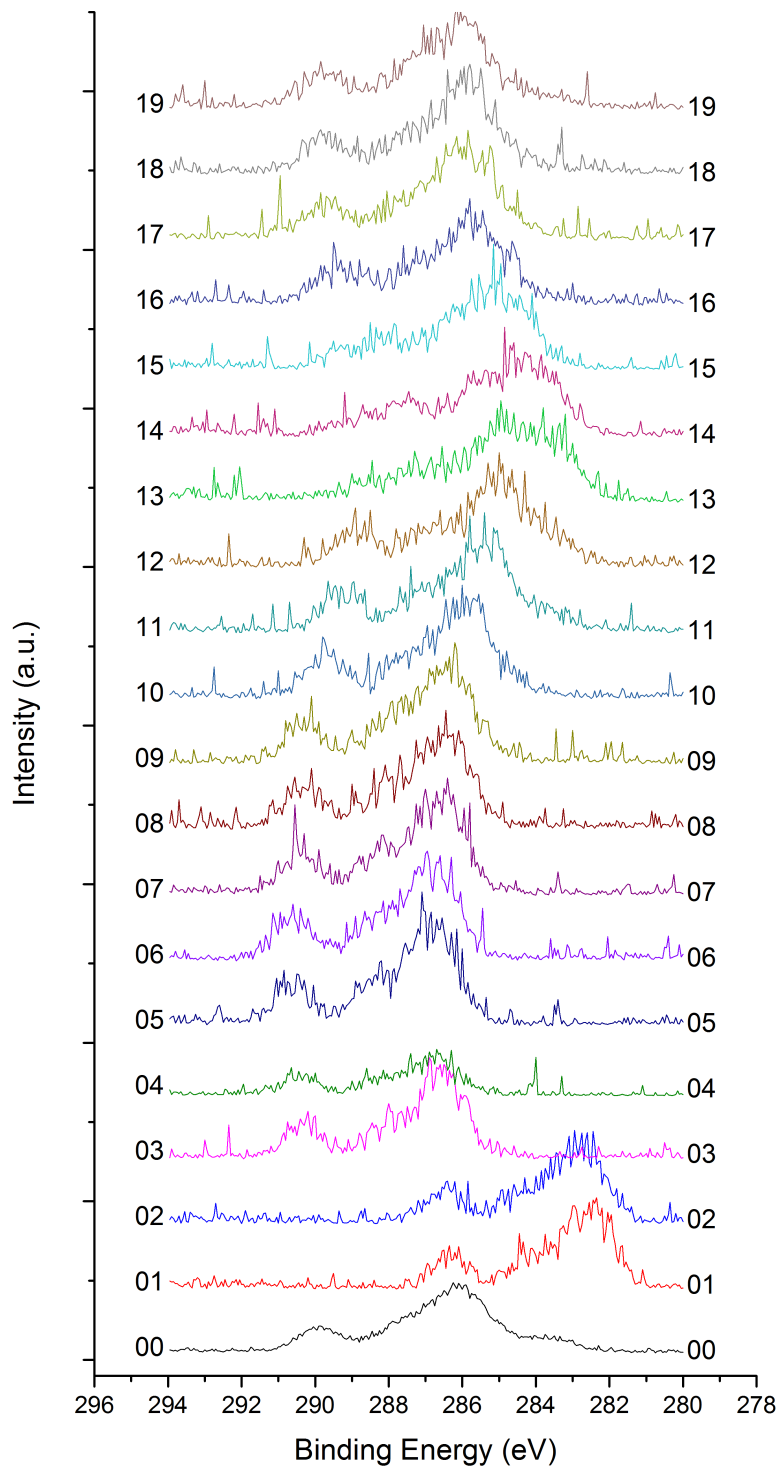


Fig. 30. The determination of flood-gun optimum by tuning the emission current of the flood-gun.

The flood-gun in the XPS chamber is used to compensate the positive charging. The current optimum of the flood-gun is determined by tuning the emission current during XPS scans. Fig. 30 shows the spectra during the measurement. At emission current lower than the optimum, the spectra shift to higher binding energy and the film is positively charged. At emission current higher than the optimum, the spectra shift to lower binding energy and the film is negatively charged. The current optimum is then measured. However, when measuring the unexposed PMMA with the flood-gun emitting at the current optimum the spectrum shows enormous peak broadening. It is probably because two processes are inducing the charge neutralization at the same time: one from the sample grounding and the other from the compensation of the flood-gun [18]. It is best to either treating the sample as insulator and using flood-gun to compensate the charge induced by X-rays, or grounding the sample that allows only the neutralization from the ground. As for the negative charge induced by electrons, there is no efficient way other than leaving the sample for a long period and wait for the charge to dissipate. For our experiments, it is very important to spin-coat the PMMA samples as thin as possible to prevent the charging.

5. Conclusions

The effects of the low-energy electrons (5 – 40 eV) irradiated on PMMA thin films on silicon wafer as a function of dose and electron energy were studied using mass spectroscopy, X-ray photoelectron spectroscopy, and atomic force microscopy. Spin-coated PMMA thin films with thickness around 40 nm are exposed with low-energy electrons. Mass spectra of mass 15, 28, 31, 44 show an energy threshold of fragmentation around 21 – 27 eV with the effects of charging. This confirms one of the fragmentation pathway that produces O-CH₃ and -C=O. The direct fragmentation of the ester group is not observed as no signal from mass 59 or 60 is seen in mass spectra during irradiation. The effect of negative charging caused by electron irradiation elevates the energy threshold above the real value.

The dissociation mechanism of PMMA is discussed and compared to literatures. The reactions that change the chemical environment of the atoms in PMMA are second-order, indicating that the reaction can be two-step. Our results fit well with the mechanism of PMMA dissociation proposed in literatures, which are studied only with high-energy e-beams or neutral irradiations. This indicates that low-energy electrons induce reactions of PMMA that similar to those induced by high-energy e-beams. Direct ionization is believed to be the main pathway of dissociation. Charge of the electrons does not induce other reactions that suggest other processes. No sign of dissociative electron attachment is observed in our result, which is possibly screened by surface charging.

The crosslinking is observed for PMMA exposed by 30 eV electrons. The dose dependence of crosslinking induced by low-energy electron is similar to those induced by high-energy e-beams. The secondary generation efficiency of 25 keV e-beam is calculated comparing the fully cross-linked dose for low-energy and high-energy exposure.

The charging effect during and after measurements causes problems that deviate the measured energies. To reduce the effect of charging, it is suggested that the PMMA films are made as thin as possible. It is also suggested that the sample is either treated as insulating sample and charge-compensated by flood-gun, or simply grounded without charge compensation.

6. References

1. Arumainayagam, C.R., et al., *Low-energy electron-induced reactions in condensed matter*. Surface Science Reports, 2010. **65**(1): p. 1-44.
2. Kozawa, T., et al., *Acid generation efficiency in a model system of chemically amplified extreme ultraviolet resist*. Journal of Vacuum Science & Technology B, 2006. **24**(6): p. L27-L30.
3. Seah, M.P. and W.A. Dench, *Quantitative electron spectroscopy of surfaces: A standard data base for electron inelastic mean free paths in solids*. Surface and Interface Analysis, 1979. **1**(1): p. 2-11.
4. Bermudez, V.M., *Low-energy electron-beam effects on poly(methyl methacrylate) resist films*. Journal of Vacuum Science & Technology B, 1999. **17**(6): p. 2512-2518.
5. Lehockey, E.M., I. Reid, and I. Hill, *Physical and chemical aspects of PMMA vapour development*. Nuclear Instruments and Methods in Physics Research Section B: Beam Interactions with Materials and Atoms, 1990. **46**(1-4): p. 364-368.
6. van Dorp, W.F., *The role of electron scattering in electron-induced surface chemistry*. (1463-9084 (Electronic)).
7. Massey, S., et al., *Chemical modification of polystyrene by low-energy (<100 eV) electron irradiation studied by mass spectrometry*. Journal of Applied Polymer Science, 2008. **108**(5): p. 3163-3168.
8. Ennis, C.P. and R.I. Kaiser, *Mechanistical studies on the electron-induced degradation of polymethylmethacrylate and Kapton*. Physical Chemistry Chemical Physics, 2010. **12**(45): p. 14902-14915.
9. Teh, W.H., et al., *Cross-linked PMMA as a low-dimensional dielectric sacrificial layer*. Microelectromechanical Systems, Journal of, 2003. **12**(5): p. 641-648.
10. Tada, T. and T. Kanayama, *Fabrication of silicon nanostructures with a poly(methylmethacrylate) single-layer process*. Journal of Vacuum Science & Technology B, 1995. **13**(6): p. 2801-2804.
11. Lehockey, E.M., I. Reid, and I. Hill, *The radiation chemistry of poly(methyl methacrylate) polymer resists*. Journal of Vacuum Science & Technology A, 1988. **6**(4): p. 2221-2225.
12. Walsh, C.B. and E.I. Franses, *Ultrathin PMMA films spin-coated from toluene solutions*. Thin Solid Films, 2003. **429**(1-2): p. 71-76.
13. Hall, D.B., P. Underhill, and J.M. Torkelson, *Spin coating of thin and ultrathin polymer films*. Polymer Engineering & Science, 1998. **38**(12): p. 2039-2045.
14. Hiraoka, H., *Radiation Chemistry of Poly(methacrylates)*. IBM Journal of Research and Development, 1977. **21**(2): p. 121-130.
15. Tinone, M.C.K., K. Tanaka, and N. Ueno, *Photodecomposition of poly(methylmethacrylate) thin films by monochromatic soft x-ray radiation*. Journal of Vacuum Science & Technology A, 1995. **13**(4): p. 1885-1892.

16. Louette, P., F. Bodino, and J.-J. Pireaux, *Poly(methyl methacrylate) (PMMA) XPS Reference Core Level and Energy Loss Spectra*. Surface Science Spectra, 2005. **12**(1): p. 69-73.
17. Gross, T., et al., *Some remarks on fitting standard- and high resolution C 1s and O 1s x-ray photoelectron spectra of PMMA*. Applied Surface Science, 1993. **68**(3): p. 291-298.
18. Yu, X.-R. and H. Hantsche, *Vertical differential charging in monochromatized small spot X-ray photoelectron spectroscopy*. Surface and Interface Analysis, 1993. **20**(7): p. 555-558.

7. Acknowledgements

It is not easy studying and living abroad. But there are persons that make it easier for me. My advisor dr. ir. W.F. van Dorp is one of them. He is not only the advisor of my master project, but also the advisor of my life during my master project. I would like to express my sincerest gratitude to him, who keeps encouraging me and spurring on me. His enthusiastic attitude shows me how a research life can be so interesting. His invaluable advices and patient guidance make all this possible. I would also like to acknowledge prof. J.T.M. De Hosson for providing me the opportunity to do my master project in Materials Science group, as well as his concern and guidance.

This project could not be done without the collaboration with dr. ir. S.J. van der Molen's group in Leiden University. I appreciate the interesting and inspiring discussions with Dr. A. Thete happened in both universities and over Skype. Together with their results I can understand my experiments better. My experiments won't be done without the equipment in the lab of the Surface and thin films group, and the facilities in the clean room of the Physics of nanodevices group.

I would like to thank L. Venema, who always answer to my problems on the technical issues, and fix up the mistakes that I made. Thanks also give to M. Dutka, D. Vainchtein, J.G. Holstein, and H.M. de Roos for their technical support. I would like to thank T. Zehra, J. Shan, L. Liang, S. Omar and other people that helped me with my experiments. I would like to thank K. Evers, J. Shen, D. Martinez-Martinez, and E. Faber and other members in materials science group for advices and discussions. Also thanks to all my schoolmates of nanoscience cohort 2012-2014, for the great time studying together.

None of this will be possible for me without my family and friends. Thanks to my parents and others who are supporting and encouraging me from far away in my home country. Thanks to M. Huang who companies me throughout my studying abroad.